Geoscience Frontiers 11 (2020) 487–494

Contents lists available at ScienceDirect

Geoscience Frontiers

journal homepage: www.elsevier.com/locate/gsf

Research Paper

Modeling the effect of wetting on the mechanical behavior of crushable granular materials

Carlos Ovalle [a,*], Pierre-Yves Hicher [b]

[a] Research Institute of Mining and Environment (RIME UQAT-Polytechnique), Department of Civil, Geological and Mining Engineering, Polytechnique Montréal, Québec, Canada

[b] GeM UMR CNRS 6183, Ecole Centrale de Nantes, France

ARTICLE INFO

Keywords:
Grain crushing
Wetting
Constitutive modeling

ABSTRACT

It is well known that the compressibility of crushable granular materials increases with the moisture content, due to the decrease of particle strength in a humid environment. An existing approach to take into account the effect of grain breakage in constitutive modeling consists in linking the evolution of the grain size distribution to the plastic work. But how the material humidity can affect this relationship is not clear, and experimental evidence is quite scarce. Based on compression tests on dry and saturated crushable sand recently reported by the present authors, a new non-linear relationship is proposed between the amount of particle breakage and the plastic work. The expression contains two parameters: (1) a material constant dependent on the grain characteristics and (2) a constant depending on the wetting condition (in this study, dry or saturated). A key finding is that the relationship does not depend on the stress path and, for a given wetting condition, only one set of parameters is necessary to reproduce the results of isotropic, oedometric, and triaxial compression tests. The relationship has been introduced into an elastoplastic constitutive model based on the critical state concept with a double yield surface for plastic sliding and compression. The breakage ratio is introduced into the expression of the elastic stiffness, the critical state line and the hardening compression pressure. Incremental stress-strain computations with the model allow the plastic work to be calculated and, therefore, the evolution of particle crushing can be predicted through the proposed non-linear relationship and reintroduced into the constitutive equations. Accurate predictions of the experimental results in terms of both stress-strain relationships and breakage ratio were obtained.

1. Introduction

Compression and shearing of granular materials under high stresses and/or large plastic strains lead to particle breakage. As a result, grading evolves to a better-graded distribution of sizes, thus increasing the compressibility for a given state of stress (Vesic and Clough, 1968; Hardin, 1985; Biarez and Hicher, 1994, 1997; Lee and Coop, 1995; Lade et al., 1996; McDowell et al., 1996; Nakata et al., 2001; Bandini and Coop, 2011; Ovalle et al., 2013). Several examples of granular materials affected by this phenomenon can be found in such engineering and geoscientific problems, involving high rockfill dams (Marsal, 1967; Frossard et al., 2012; Ovalle et al., 2014, 2015a; Xiao et al., 2018), pile penetration, granular fills in discontinuities of rock masses (Sammis et al., 1986), rock fragmentation by weathering, formation of glacial till (Turcotte, 1986), subsidence of fractured rock deposits (Zhang and Buscarnera, 2017), etc.

The fracturing of an individual loaded grain occurs through the propagation of existing microcracks within the solid particle. The resistance of crack propagation depends on both the grain characteristics (mineralogy, size) and weathering, whereas the loading condition of the particle depends on external loads and material parameters such as particle shape, grain size distribution (gsd), packing density, and granular fabric. It is also well known that a humid environment corrodes the tip of microcracks, which causes a decrease of the crack propagation resistance (Atkinson, 1982; Dunning et al., 1984; Oldecop and Alonso, 2007). Therefore, environmental conditions play a crucial role on the mechanical response of crushable granular materials; for a given state of stress, the higher the material humidity, the higher the amount of particle crushing and the compressibility (Oldecop and Alonso, 2003; Ovalle, 2013). Moreover, several studies have shown that flooding a dry sample under constant stress lead to collapse triggered by particle crushing

* Corresponding author. Polytechnique Montréal (Room A-356), 2900 Edouard Montpetit Blvd, Montreal, QC, H3T 1J4, Canada.
E-mail address: carlos.ovalle@polymtl.ca (C. Ovalle).
Peer-review under responsibility of China University of Geosciences (Beijing).

https://doi.org/10.1016/j.gsf.2019.06.009
Received 19 April 2018; Received in revised form 15 April 2019; Accepted 13 June 2019
Available online 12 July 2019

(Nobari and Duncan, 1972; Lee and Coop, 1995; Oldecop and Alonso, 2001; Ovalle et al., 2015b).

A number of authors have shown through experimentation that the plastic work (w_p) in loaded crushable granular materials is related to the evolution of the gsd (Miura and O-Hara, 1979; Daouadji et al., 2001; Ovalle et al., 2013). Therefore, a proper definition of the amount of particle breakage can be used as an energy dissipation parameter in constitutive models (Daouadji et al., 2001; Einav, 2007; Daouadji and Hicher, 2010; Hu et al., 2011, 2018; Liu et al., 2017; Xiao and Liu, 2017; Yin et al., 2017; Dano et al., 2018). However, the role of the material humidity in the relationship between w_p and the amount of particle breakage has not been widely discussed. A better understanding of this issue could enhance the existing models so that the effect of wetting in crushable materials could be taken into account.

In this paper, an expression relating the particle breakage ratio and the plastic work is proposed based on experimental data of isotropic, oedometric, and triaxial compression tests on dry and saturated crushable sand. The non-linear relationship contains two parameters: one is a material constant which depends on the grain characteristics and the second is linked to the wetting condition, dry or saturated in the present study. Then, an elastoplastic constitutive model is used to predict the plastic work at any stress level and the theoretical breakage ratio can be obtained through the proposed expression. The model takes into account the material degradation due to particle crushing on the elastic stiffness, the critical state line, and the hardening pressure, by calculating the predicted breakage ratio at each stress increment. Published results on dry and saturated sand were used to calibrate and validate the model.

2. Experimental testing

With the aim of exploring the effect of the material humidity on the relationship between the amount of particle breakage and w_p, data previously published by the authors (Ovalle et al., 2015b) were analyzed in this study. The authors carried out a comprehensive experimental program on uniform sand with particles sized from 2 to 2.5 mm, obtained from sieving a grinded quartzite shale rock from the Trois Vallées quarry in the north of France. Isotropic, oedometric and triaxial drained compression tests were conducted on loose samples in a constant climate chamber at 20 °C and 60% of relative humidity. Three different sets of tests were performed, called D, S, and F in Table 1:

(1) D: tests on air dried samples in the climate chamber;
(2) S: tests on saturated samples flooded with demineralized water before the initial loading stage;
(3) F: tests on air dried samples flooded with demineralized water at a given constant stress.

Due to the uniform initial grading and angular particle shape, the authors obtained scatter on the void ratio at sample preparation of about 1.00 ± 0.07; an average initial void ratio of 1.0 has been assumed in all simulations presented later in this paper. All samples were sieved after testing in order to study the evolution of grading under a variety of stress paths, stress magnitudes, and wetting conditions (i.e., dry for D and saturated for S and F). Table 1 contains the set of analyzed tests; more details concerning the material and samples preparation can be found in Ovalle et al. (2015b). S tests were conducted under drained condition; the results can therefore be expressed in terms of effective stresses. Concerning D tests and F tests before flooding, the pores were saturated by air at 60% of relative humidity and it is assumed that suction in capillary bridges at inter-granular contacts is negligible, which is generally the case in coarse sands; therefore, the results are also analyzed in terms of effective stresses.

Several definitions for a particle breakage index have been suggested in previous studies, typically based on a ratio depending on the initial and an assumed ultimate gsd (Einav, 2007; Hardin, 1985; Lade et al., 1996). Experimental data have shown that the ultimate gsd in materials under large stress and/or strains evolves to a fractal distribution given by Nakata el al. (2001), Coop et al. (2004), and Einav (2007).

$$F_u(d) = (d/d_{\max})^{3-D} \tag{1}$$

where the exponent D is called the fractal dimension, d is the particle size and $d_{\max}$ is the size of the coarsest grain. Similarly, observations of rock fragmentation under high energy conditions (e.g. explosions, formation of glacial till, cataclasis in the formation of fault gouge) have shown that the gsd evolves also towards a fractal distribution, where D is typically between 2.5 and 2.7 (Sammis et al., 1986; Turcotte, 1986). Einav (2007) has used these findings in order to define a breakage index B_r computed as the ratio between the area flanked by the initial gsd and any intermediate gsd after crushing, and the area flanked by the initial gsd and the ultimate fractal distribution given by Eq. (1). Therefore, B_r varies

Table 1
Experimental data for model calibration and validation.

Test N°	Initial void ratio	σ'_{v-max} or σ'_3 (MPa) (*)	B_r	w_p (MPa)	Test conditions
Triaxial tests					
D1 (†)	0.933	0.80	0.22	0.372	Dry
F3	0.935	0.80	0.25	0.345	Flooded after isotropic consolidation
D7	0.949	0.40	0.17	0.199	Dry
Isotropic tests					
D9	1.069	0.40	0.04	0.010	Dry
D10	0.955	0.80	0.06	0.019	Dry
F11	0.991	0.40	0.04	0.009	Flooded at $\sigma'_3 = 0.4$ MPa
F12	0.952	0.80	0.08	0.018	Flooded at $\sigma'_3 = 0.8$ MPa
Oedometric tests					
D14	1.066	0.40	0.06	0.033	Dry
D15	1.015	0.60	0.07	0.032	Dry
D16	0.995	0.80	0.08	0.040	Dry
D17 (†)	1.014	2.10	0.13	0.118	Dry
D18	0.990	2.10	0.14	0.123	Dry
S19	1.035	0.40	0.08	0.016	Saturated
S20	1.029	0.80	0.12	0.046	Saturated
S21 (†)	1.051	2.10	0.22	0.174	Saturated
F22 (†)	1.008	2.10	0.21	0.173	Flooded at $\sigma'_v = 0.40$ MPa and reloaded to 2.1 MPa
F23	1.009	0.40	0.08	0.018	Flooded at $\sigma'_v = 0.40$ MPa
F24	1.000	0.85	0.12	0.052	Flooded at $\sigma'_v = 0.85$ MPa
F25 (†)	1.003	2.10	0.21	0.201	Flooded at $\sigma'_v = 1.50$ MPa and reloaded to 2.1 MPa

(*) σ'_{v-max} for oedometric tests and σ'_3 for isotropic and triaxial tests.
(†) Tests used only for model validation.

between 0, for no crushing, and 1, when the ultimate state is reached. Here, the definition of Einav (2007) is used, assuming $D = 2.5$.

Table 1 includes the values of B_r for all tests analyzed in this paper. Fig. 2 shows the experimental results of B_r as a function of the mean effective pressure (p') and the stress ratio (η), defined as $p' = (\sigma_1' + 2\sigma_3')/3$ (assuming a constant ratio $\sigma_3'/\sigma_1' = 0.5$ in oedometric tests), $\eta = q/p'$ and the deviatoric stress $q = \sigma_1' - \sigma_3'$. As expected, the amount of particle breakage increases with the material humidity and the stress ratio.

3. Linking particle breakage and plastic work

As shown by Ovalle et al. (2015b), if the experimental data are plotted in terms of B_r against w_p, the relationship depends only on the wetting condition, regardless of the stress path. This finding suggests that a two parameter expression relating B_r and w_p could be appropriate for modeling the effect of wetting, where a first parameter defines the grain characteristics and the second one the wetting condition. The proposed relationship between B_r and w_p is given by

$$B_r = \left(\frac{w_p}{a + w_p}\right)^c \tag{2}$$

where a is a material constant and c depends on the wetting condition. Following Yin et al. (2017), the formulation of the plastic work is written as

$$w_p = \int \left(p' < d\varepsilon_v^p > + q d\varepsilon_d^p\right) \tag{3}$$

where $d\varepsilon_v^p$ and $d\varepsilon_d^p$ are the volumetric and deviatoric plastic strain increments, respectively. The MacCauley function $\langle d\varepsilon_v^p \rangle$ in Eq. (3) suggests that particle breakage occurs only during shear induced contraction. Fig. 1a shows plots of Eq. (2) for a constant parameter a and range of values for c. It can be seen that c controls the magnitude of the plastic work at which particle crushing starts; *i.e.* c defines the onset of crushing. On the other hand, Fig. 1b indicates that, for a given value of c, the parameter a controls the evolution of particle crushing during loading. As

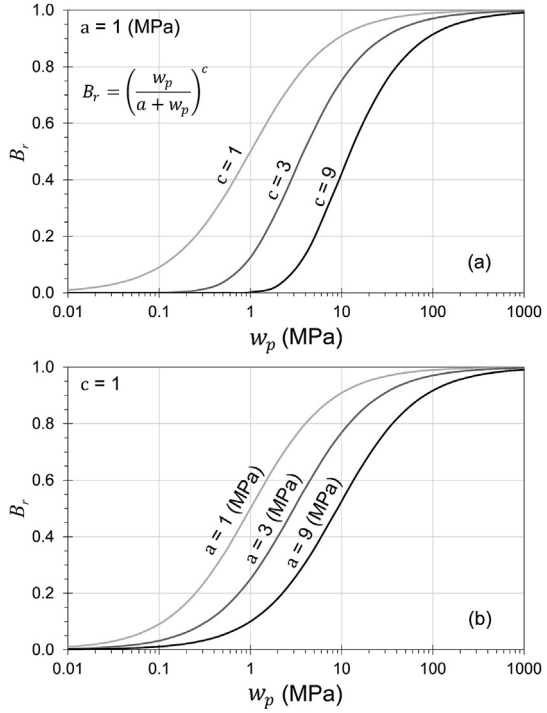

Fig. 1. Proposed relationship B_r versus w_p and effect of parameters a and c.

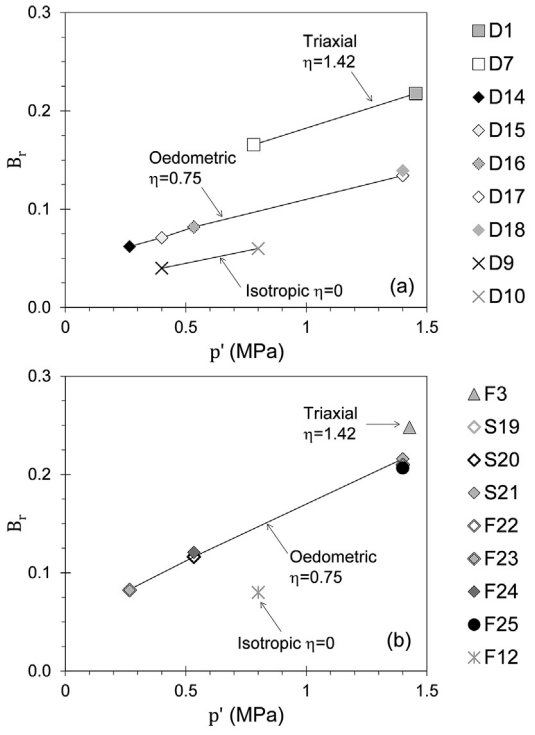

Fig. 2. B_r versus mean effective pressure after isotropic, oedometric and triaxial tests on (a) D and (b) S and F samples.

aforementioned, at high stress and/or large strain (i.e. high w_p) the amount of particle breakage evolves to an ultimate state characterized by a fractal distribution of constant exponent D in Eq. (1) (Coop et al., 2004). According to the definition of B_r (Einav, 2007), this means that B_r should evolve asymptotically to 1 at large w_p, which is properly captured by the shape of Eq. (2).

Fig. 3a presents the fitting of Eq. (2) to the experimental results used for calibration. A closer examination of the experimental values in Fig. 3b

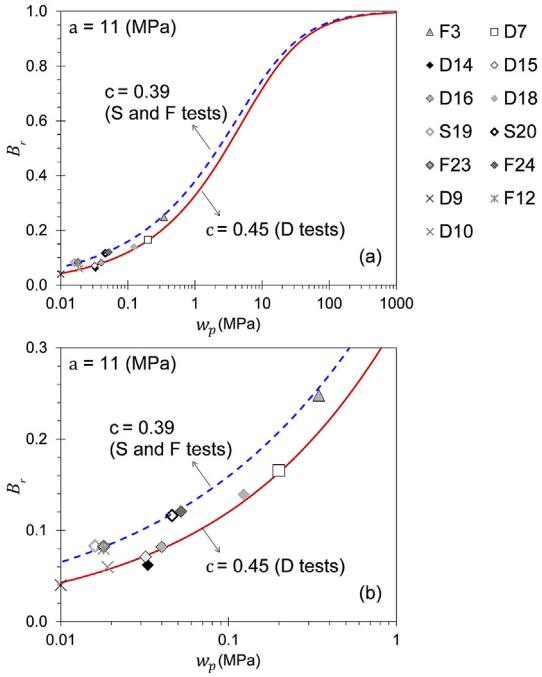

Fig. 3. Calibration of parameters a and c.

indicates that wetted samples (S and F tests) present higher B_r at a given w_p and can be represented by a separate curve compared to dry ones (D tests). A good agreement between Eq. (2) is obtained by adopting a material parameter $a = 11$ MPa, with $c = 0.39$ and 0.45 for wetted and dry samples, respectively. In this work, most of the experimental data in Fig. 3 is in the low range of B_r and w_p; however, other authors have shown that a similar relation (with only 1 parameter a, i.e. with $c = 1$) is valid for values up to more than $w_p = 10$ MPa (Dano et al., 2018; Hu et al., 2018, 2011). Hereafter, Eq. (2) is introduced within an elastoplastic model. The plastic work is computed at each incremental loading step and the obtained value of B_r is introduced into the constitutive equations.

4. Elastoplastic constitutive model

Eq. (2) is introduced into the elastoplastic model proposed by Yin et al. (2017), with the aim of accounting for the effect of wetting in crushable materials. The original model considers the effect of particle breakage based on the critical state concept by an approach previously developed by Daouadji et al. (2001), Muir Wood et al. (2009), Daouadji and Hicher (2010), Hu et al. (2011), among others. Yin et al. (2017) used the one parameter relationship of B_r against w_p, originally proposed by Hu et al. (2011) in order to predict the evolution of grading during grain crushing. Here, the two parameter expression in Eq. (2) has been introduced in the model with the aim of modeling the effect of wetting.

The total strain increment is conventionally composed of both elastic and plastic strain rates:

$$\dot{\varepsilon}_{ij} = \dot{\varepsilon}^e_{ij} + \dot{\varepsilon}^p_{ij} \tag{4}$$

4.1. Non-linear elasticity

The elastic bulk modulus (K) and the shear modulus (G) are considered to be non-linear, depending on the mean effective stress and the void ratio (Richart et al., 1970). Iwasaki and Tatsuoka (1977) showed that the elastic stiffness decreases when the gsd becomes wider. Yin et al. (2017) took into account this effect by defining K and G depending on B_r by the following expressions:

$$\begin{aligned} K &= K_0 \cdot p_{at} \frac{(2.97-e)^2}{(1+e)} \left(\frac{p'}{p_{at}}\right)^n \exp(-\rho B_r) \\ G &= G_0 \cdot p_{at} \frac{(2.97-e)^2}{(1+e)} \left(\frac{p'}{p_{at}}\right)^n \exp(-\rho B_r) \end{aligned} \tag{5}$$

where K_0, G_0 and n are material constants, $p_{at} = 101.3$ kPa is the atmospheric pressure, and the parameter ρ controls the stiffness degradation rate. Following Yin et al. (2017), $\rho = 0.94$ was assumed. Volumetric ($\dot{\varepsilon}^e_v$) and deviatoric ($\dot{\varepsilon}^e_d$) elastic strain increments are obtained as follows:

$$\dot{\varepsilon}^e_v = \frac{\dot{p'}}{K} \quad \text{and} \quad \dot{\varepsilon}^e_d = \frac{\dot{q}}{3G} \tag{6}$$

4.2. Plastic behavior

The model has two yield surfaces f_s and f_c, for shear sliding and compression, respectively; the plastic strain increment can be expressed as

$$\dot{\varepsilon}^p_{ij} = \dot{\varepsilon}^{p_s}_{ij} + \dot{\varepsilon}^{p_c}_{ij} \quad \text{where} \quad \begin{cases} \dot{\varepsilon}^{p_s}_{ij} = d\lambda_s \dfrac{\partial g_s}{\partial \sigma'_{ij}} \\ \dot{\varepsilon}^{p_c}_{ij} = d\lambda_c \dfrac{\partial g_c}{\partial \sigma'_{ij}} \end{cases} \tag{7}$$

$d\lambda_s$ and $d\lambda_c$ are the plastic multipliers depending on the stress increment and on plastic hardening laws, g_s and g_c are the plastic potentials for shear sliding and compression, respectively, and $f_{s,c} < 0$ implies $d\lambda_{s,c} = 0$.

4.2.1. Plastic-sliding

The shear sliding yield function f_s is defined as

$$f_s = \frac{q}{p'} - H_s \tag{8}$$

H_s is the hardening parameter given by

$$H_s = \frac{M_p \varepsilon^p_d}{\frac{M_p p'}{G_{pR} G} + \varepsilon^p_d} \tag{9}$$

where G_{pR} is the relative plastic stiffness and M_p is the stress ratio mobilized at the peak friction angle (φ_p):

$$M_p = \frac{6\sin\varphi_p}{3-\sin\varphi_p} \tag{10}$$

The plastic potential function g_s is given by

$$g_s = \frac{q}{M_{pt} p'} + \ln(p') \tag{11}$$

where M_{pt} is the stress ratio mobilized at the phase transformation angle (φ_{pt}):

$$M_{pt} = \frac{6\sin\varphi_{pt}}{3-\sin\varphi_{pt}} \tag{12}$$

The plastic multiplier $d\lambda_s$ from Eq. (7) can be obtained by replacing $\dot{\varepsilon}^{p_s}_d = d\lambda_s \frac{\partial g_s}{\partial q}$ in the following consistency condition equation:

$$\frac{\partial f_s}{\partial \sigma'_{ij}} \dot{\sigma}'_{ij} + \frac{\partial f_s}{\partial H_s} \cdot \frac{\partial H_s}{\partial \varepsilon^p_d} \dot{\varepsilon}^{p_s}_d = 0 \tag{13}$$

4.2.2. Critical state

The model is based on the critical state concept, defined as a state of constant volume and constant effective stress at large shear strain. The Critical State Line (CSL) in the $e-\ln p'$ plane gives the critical void ratio e_c as follows:

$$e_c = e_{\text{ref}} - \lambda \ln\left(\frac{p'}{p_{\text{ref}}}\right) \tag{14}$$

where λ is the slope of the CSL, while e_{ref} and p_{ref} are the coordinates of a reference point located on the CSL. The approach to model increasing compressibility due to particle breakage consists in parallel shifting down the CSL toward lower values of e when B_r increases (Biarez and Hicher, 1997; Daouadji et al., 2001; Muir Wood and Maeda, 2008; Bandini and Coop, 2011; Li et al., 2014; Xiao et al., 2016). Therefore, if a constant e_{ref} is assumed, a variable p_{ref} could be used to take into account this effect. In this study, a fixed value $e_{\text{ref}} = 0.66$ is assumed and p_{ref} is given by the following expression:

$$p_{\text{ref}} = p_{\text{ref}_0} \exp(-bB_r) \tag{15}$$

where the parameter b controls the rate of the CSL shift caused by grain breakage and $p_{\text{ref}_0} = 1$ MPa. Since the location of the CSL can be assumed to be dependent only on the current gsd after breakage (Biarez and Hicher, 1997), b is assumed to be a material constant, regardless of the wetting condition.

The model considers fully shear sliding mobilization in loose packings of constant friction angle at critical state (φ_μ). The previous statement means that, according to experimental evidence (Coop et al., 2004), φ_μ remains constant when B_r increases. As shown by Xiao et al. (2019), this would not be the case if the particle shape varies during particle breakage, however this is not considered in this model. In dense

packings, the peak friction angle (φ_p) before critical state is obtained as (Chang and Hicher, 2005)

$$\tan\varphi_p = \left(\frac{e_c}{e}\right)\tan\varphi_\mu \tag{16}$$

Thus, after the phase transformation state, the granular assembly starts to dilate; the peak friction angle is reduced, resulting in strain softening. The phase transformation angle φ_{pt} also depends on the packing density and is expressed as (Chang and Hicher, 2005)

$$\tan\varphi_{pt} = \left(\frac{e_c}{e}\right)^{-1}\tan\varphi_\mu \tag{17}$$

which means that a dense packing has a lower phase transformation angle than does a loose packing.

The whole formulation implies that dilatancy decreases with particle crushing.

4.2.3. Compression behavior

The compression behavior is given by an associate flow rule and the following yield surface proposed by Kikumoto et al. (2010) is adopted:

$$f_c = \frac{1}{2}\left(\frac{\eta}{M_p}\right)^3 p' + p' - p_m \quad for\ \eta \le M_p \tag{18}$$

The yield surface expands with the plastic volumetric strain by means of the evolution of the hardening variable p_m, where the influence of particle breakage is incorporated through B_r as follows:

$$p_m = p_{m_0}\exp\left(\frac{1+e_o}{\lambda-\kappa}\varepsilon_v^p\right)\exp(-b' B_r) \tag{19}$$

where $\kappa = \lambda/10$ is assumed.

The plastic multiplier $d\lambda_c$ from Eq. (7) can be obtained by replacing $\dot{\varepsilon}_v^{p_c} = d\lambda_c\frac{\partial g_c}{\partial p}$ in the following consistency condition equation:

$$\frac{\partial f_c}{\partial \sigma'_{ij}}\dot{\sigma}'_{ij} + \frac{\partial f_c}{\partial p_m}\cdot\frac{\partial p_m}{\partial \varepsilon_v^p}\dot{\varepsilon}_v^{p_c} = 0 \tag{20}$$

The original model of Yin et al. (2017) considered that b in Eq. (15) and b' in Eq. (19) were the same parameter; in other words, the same rate of shifting was imposed for compression hardening and for the CSL. As the CSL is related to the current gsd after particle crushing regardless of the process of breakage which previously occurred (Biarez and Hicher, 1997; Li et al., 2013, 2014), b is considered a material constant in this study. On the other hand, the compression hardening depends on the wetting condition (Ovalle, 2018), because particle crushing is promoted at high humidity. Thus, p_m is reduced when the humidity increases, which means that b' is not a material constant but depends on the wetting condition.

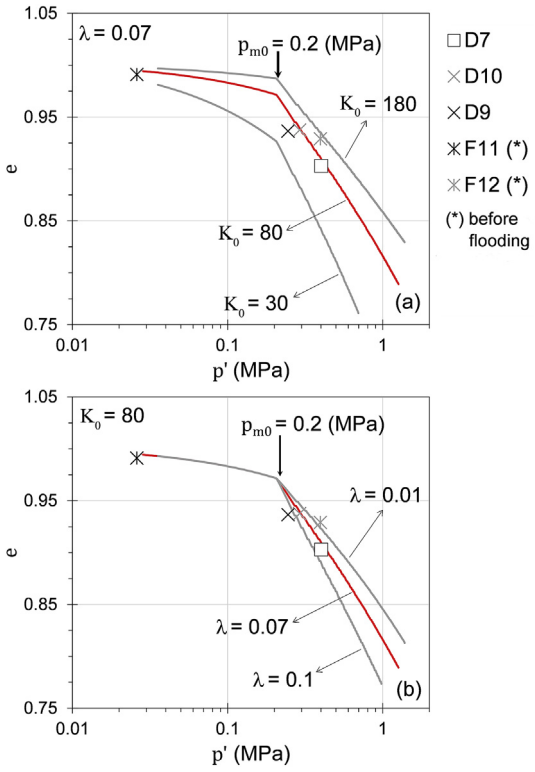

Fig. 4. Model calibration on isotropic compression tests.

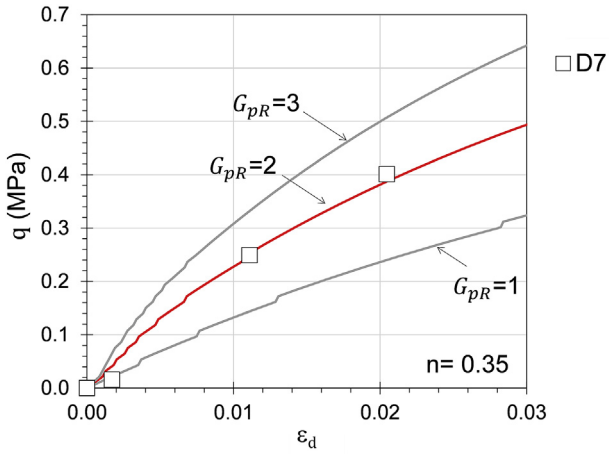

Fig. 5. Calibration of elastic parameters.

5. Model calibration and validation

The calibration of the model parameters was based on the set of tests presented in Table 1, except for tests D1, D17, S21, F22 and F25, which were used only for modeling validation, as shown later in the paper. Eq. (2) (see Fig. 3) was introduced into the model in order to obtain B_r after each simulated stress increment. Fig. 4 presents the calibration of K_0, λ and p_{m_0} using isotropic compression tests on dry samples (F tests before flooding); G_0 was obtained assuming a constant Poisson's ratio $\nu = 0.25$. The calibration of n and G_{pR} is shown in Fig. 5 for dry test D7, using data for shear strain levels up to $\varepsilon_d = 2\%$. Provided that typical values of n are in the range of 0.3–0.4 (Chang and Hicher, 2005; Hu et al., 2011; Yin et al., 2017), a constant value $n = 0.35$ was used for the calibration of $G_{pR} = 2$ (see Fig. 5).

According to test D7, the critical state in the stress plane is given by a friction angle $\varphi_\mu = 35°$. Increasing compressibility due to particle breakage through the shifting of the CSL is reached using a material parameter $b = 10$ based on test F3. The effect of breakage in the hardening law for the compression behavior is given by b', controlling the rate of increase of the yield surface f_c. After calibration, b' was found equal 10 and 1 for test F3 (flooded) and D7 (dry), respectively. Fig. 6 presents the calibration using triaxial tests F3 and D7; a model validation for dry test D1 is also included. Model validation of the set of determined parameters is shown in Fig. 7 through the simulation of oedometric compression tests on dry and saturated samples, showing a good agreement with the experimental results.

In order for the collapse after flooding dry compressed sand to be modeled, the following strategy was adopted:

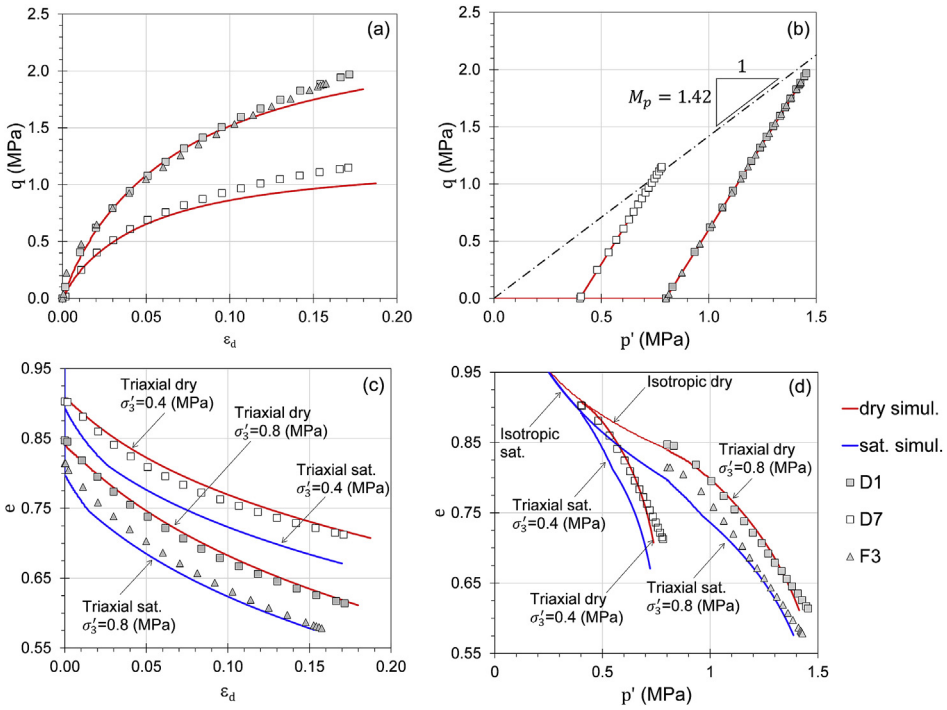

Fig. 6. Model simulation of triaxial tests on dry and saturated samples.

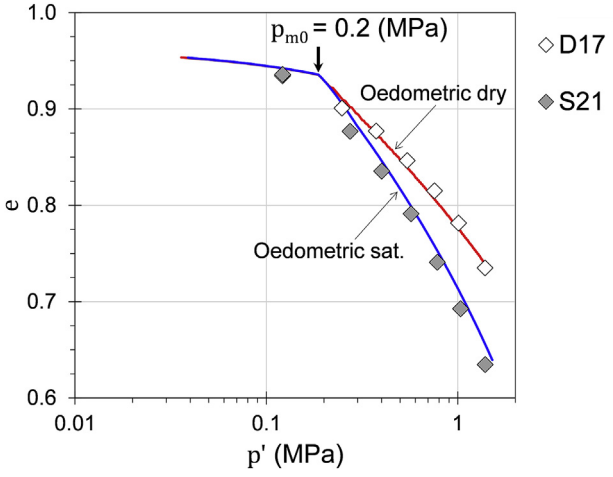

Fig. 7. Validation for oedometer tests.

Table 2
Model parameters.

Group	Parameter	Values
Elastic parameters	K_0	80
	G_0	48
	n	0.35
	ρ	0.94
Plastic parameters	G_{pR}	2.0
	p_{m_0} (MPa)	0.2
	φ_μ (°)	35
Critical state	p_{ref_0} (MPa)	1.0
	e_{ref}	0.66
	λ	0.07
Grain breakage	a (MPa)	11
	b	10
	c (dry)	0.45
	c (saturated)	0.39
	b' (dry)	1
	b' (saturated)	10

(1) Test simulation of a dry sample using the set of parameters previously calibrated from dry tests ($c = 0.45$ and $b' = 1$ in Table 2), up to a given constant stress state.
(2) Then, the flooding of the specimen at constant stress is simulated by modifying c and b' to the values previously calibrated from saturated tests; i.e., c varies from 0.45 to 0.39, and b' from 1 to 10, which implies a reduction of the elastic region limited by f_c. The other parameters remain unchanged. In order for a constant stress during flooding to be maintained, f_c has to be updated by an increase of the plastic strains given by $\dot{\varepsilon}_{ij}^{p_c} = d\lambda_c \frac{\partial g_c}{\partial \sigma_{ij}}$, while $\dot{\varepsilon}_{ij}^{p_s} = 0$, and the elastic strain increments are null during this stage.
(3) Thus, the plastic strain has to evolve until the new hardening pressure p_m reaches the value previously obtained just before flooding. The plastic volumetric strains computed during this process will result in the collapse of the specimen at constant stress. This process also involves an increase of w_p, and, therefore, B_r also grows, affecting the model response.

Following the aforementioned strategy, Fig. 8 presents the validation of the model through the simulation of oedometric tests F22 and F25, flooded at constant vertical stresses of 0.85 and 2.1 MPa, respectively. The numerical results appear to agree both qualitatively and quantitatively with the experimental data. Finally, Fig. 9 presents a suitable agreement between experimental and predicted values of B_r for different loading conditions, where none of the tests were used for calibration.

6. Conclusions

Previous studies have shown that, for a given stress path, particle breakage and the compressibility of crushable granular materials increase with the material humidity. Based on experimental data of a variety of loading paths on dry and saturated crushable sand with a given initial uniform grading, a new relationship linking the breakage ratio and the plastic work is suggested. For a given material, this relationship depends only on the wetting condition, regardless of the stress path, suggesting that it can be introduced into a constitutive model in order to

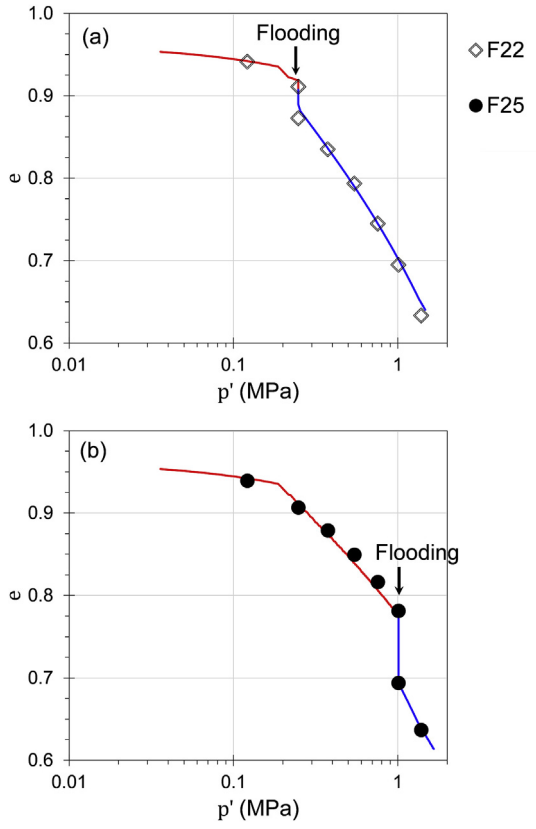

Fig. 8. Simulation of flooding and collapse in oedometer tests.

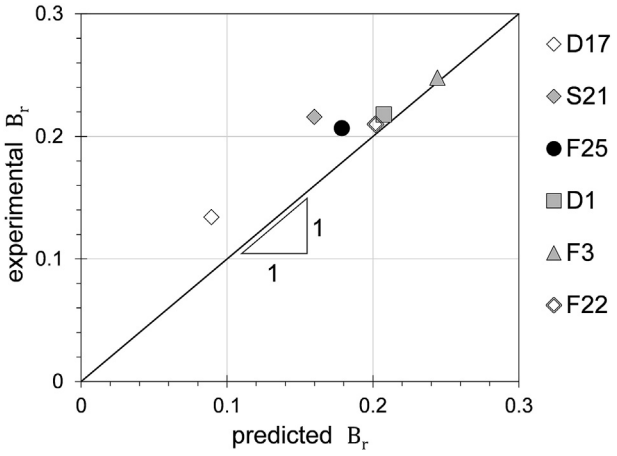

Fig. 9. Experimental against predicted B_r.

predict the amount of particle breakage and its evolution along any stress path.

An elastoplastic model based on the critical state theory with a double yield surface (shearing and compression) was used for this purpose. The model takes into account the increasing compressibility during particle breakage through a critical state line that shifts towards lower values of *e* in the void ratio–mean effective stress plane, while the critical friction angle stays constant. Thus, the shearing yield surface remains unchanged with particle crushing, while the hardening pressure of the compression yielding decreases, thereby generating additional plastic strains if crushing increases. Therefore, for the material behavior to be accurately captured, the amount of particle breakage must evolve at each stress and strain increment. This can be obtained by introducing the computed plastic work linked to the breakage ratio in the new proposed relation.

The predictions of the model in terms of both strain-stress response and evolution of the breakage ratio appear to be in good agreement with the experimental results. This means that the evolution of the grain size distribution can be predicted.

In this study only dry and saturated tests have been considered. This work can now be extended to model the influence of partial saturation, which could easily be done by calibrating the parameter *b*' within the interval of values obtained for dry and saturated conditions (i.e. $1 < b' < 10$ for the material used here). That is to say, every partial saturation condition should have a different *b*'. Another extension of this work may be to enhance the model formulation in order to take into account the creep behavior due to delayed particle crushing events.

Acknowledgements

This research work benefitted from the financial support of CONICYT Chile through project FONDECYT 11150084.

References

Atkinson, B., 1982. Subcritical crack propagation in rocks: Theory, experimental results and applications. J. Struct. Geol. 4 (1), 41–56.
Bandini, V., Coop, M.R., 2011. The influence of particle breakage on the location of the critical state line of sands. Soils Found. 51 (4), 591–600.
Biarez, J., Hicher, P.Y., 1994. Elementary mechanics of soil behaviour. Balkema, Rotterdam.
Biarez, J., Hicher, P.Y., 1997. Influence de la granulométrie et de son évolution par ruptures de grains sur le comportement mécanique de matériaux granulaires. Rev. Fr. Génie Civ. 1 (4), 607–631 (in French).
Chang, C.S., Hicher, P.-Y., 2005. An elasto-plastic model for granular materials with microstructural consideration. International J. Solids Struct. 42, 4258–4277.
Coop, M.R., Sorensen, K.K., Bodas Freitas, T., Georgoutsos, G., 2004. Particle breakage during shearing of a carbonate sand. Géotechnique 54 (3), 157–163.
Dano, C., Ovalle, C., Yin, Z., Daouadji, A., Hicher, P.-Y., 2018. Behavior of granular materials affected by grain breakage. In: Nicot, F., Millet, O. (Eds.), Advances in multi-physics and multi-scale couplings in geo-environmental mechanics, 1st ed. ISTE Press., pp. 95–132
Daouadji, A., Hicher, P.-Y., 2010. An enhanced constitutive model for crushable granular materials. Int. J. Numer. Anal. Methods Geomech. 34 (6), 555–580.
Daouadji, A., Hicher, P.-Y., Rahma, A., 2001. An elastoplastic model for granular materials taking into account grain breakage. Eur. J. Mech. A: Solids 20, 113–137.
Dunning, J., Petrovski, D., Schuyler, J., Owens, A., 1984. The effects of aqueous chemical environments on crack propagation in quartz. J. Geophys. Res. 89 (B6), 4115–4123.
Einav, I., 2007. Breakage mechanics- Part I: Theory. J. Mech. Phys. Solids 55 (6), 1274–1297.
Frossard, E., Hu, W., Dano, C., Hicher, P.Y., 2012. Rockfill shear strength evaluation: A rational method based on size effects. Géotechnique 62 (5), 415–428.
Hardin, B.O., 1985. Crushing of soil particles. J. Geotech. Eng. 111 (10), 1177–1192.
Hu, W., Yin, Z., Dano, C., Hicher, P.-Y., 2011. A constitutive model for granular materials considering grain breakage. Sci. China Technol. Sci. 54, 1–9.
Hu, W., Yin, Z., Scaringi, G., Dano, C., Hicher, P.-Y., 2018. Relating fragmentation, plastic work and critical state in crushable rock clasts. Eng. Geol. 246, 326–336.
Iwasaki, T., Tatsuoka, F., 1977. Effects of grain size and grading on dynamic shear moduli of sands. Soils Found. 17 (3), 19–35.
Kikumoto, M., Wood, D.M., Russell, A., 2010. Particle crushing and deformation behaviour. Soils Found. 50 (4), 547–563.
Lade, P., Yamamuro, J., Bopp, P., 1996. Significance of particle crushing in granular materials. J. Geotech. Eng. 122 (4), 309–316.
Lee, I., Coop, M., 1995. The intrinsic behaviour of a decomposed granite soil. Géotechnique 45 (1), 117–130.
Li, G., Liu, Y., Dano, C., Hicher, P., 2014. Grading-dependent behavior of granular materials: From discrete to continuous modeling. J. Eng. Mech. 141 (6), 04014172, 1-15.
Li, G., Ovalle, C., Dano, C., Hicher, P.-Y., 2013. Influence of grain size distribution on critical states of granular materials. In: Yang, Q., et al. (Eds.), Constitutive modeling of geomaterials. Springer series in geomechanics and geoengineering. Springer, pp. 207–210.
Liu, M., Zhang, Y., Zhu, H., 2017. 3D elastoplastic model for crushable soils with explicit formulation of particle crushing. J. Eng. Mech. 143 (12), 04017140.
Marsal, R., 1967. Large-scale testing of rockfill materials. J. Soil Mech. Found. Div. ASCE 93 (SM2), 27–44.
McDowell, G.R., Bolton, M.D., Roberston, D., 1996. The fractal crushing of granular materials. J. Mech. Phys. Solids 44 (12), 2079–2102.
Miura, N., O-Hara, S., 1979. Particle-crushing of a decomposed granite soil under shear stresses. Soils Found. 19 (3), l–14.
Muir Wood, D., Kikumoto, M., Russell, A.R., 2009. In: Oka, F., Murakami, A., Kimoto, S. (Eds.), Particle crushing and deformation behaviour. Prediction and simulation methods for geohazard mitigation. CRC Press, London.
Muir Wood, D., Maeda, K., 2008. Changing grading of soil: Effect on critical states. Acta Geotech. 3, 3–14.

Nakata, Y., Hyodo, M., Hyde, A.F.L., Kato, Y., Murata, H., 2001. Microscopic particle crushing of sand subjected to high pressure one-dimensional compression. Soils Found. 41 (1), 69–82.
Nobari, E.S., Duncan, J.M., 1972. Effect of reservoir filling on stresses and movements in earth and rockfill dams, Department of Civil Engineering. University of California. Report No. TE-72-1.
Oldecop, L., Alonso, E., 2001. A model for rockfill compressibility. Géotechnique 51 (2), 127–139.
Oldecop, L., Alonso, E., 2003. Suction effects on rockfill compressibility. Géotechnique 53 (2), 289–292.
Oldecop, L., Alonso, E., 2007. Theoretical investigation of the time dependent behavior of rockfill. Géotechnique 57 (3), 289–301.
Ovalle, C., 2013. Contribution à l'étude de la rupture des grains dans les matériaux granulaires. Doctoral thesis, École Centrale de Nantes, France (in French).
Ovalle, C., 2018. Role of particle breakage in primary and secondary compression of wet and dry sand. Géotech. Lett. 8 (2), 161–164.
Ovalle, C., Bard, E., Dano, C., Hicher, P.-Y., Dorador, L., Campaña, J., et al., 2015a. A review of large triaxial tests on coarse rockfills. From Fundamentals to Applications in Geotechnics. In: 5th pan-American conference on soil mechanics and geotechnical engineering, buenos aires, November 15 to 18, 2015. 1, pp. 3256–3263.
Ovalle, C., Dano, C., Hicher, P.-Y., 2013. Experimental data highlighting the role of surface fracture energy in quasi-static confined comminution. Int. J. Fract. 182 (1), 23–130.
Ovalle, C., Dano, C., Hicher, P.-Y., Cisternas, M., 2015b. Experimental framework for evaluating the mechanical behavior of dry and wet crushable granular materials based on the particle breakage ratio. Can. Geotech. J. 52 (5), 587–598.
Ovalle, C., Frossard, E., Dano, C., Hu, W., Maiolino, S., Hicher, P.-Y., 2014. The effect of size on the strength of coarse rock aggregates and large rockfill samples through experimental data. Acta Mech. 225, 2199–2216.
Richart, F.E., Hall, J.R., Woods, R.D., 1970. Vibrations of soils and foundations. International series in theoretical and applied mechanics. Prentice-Hall, Englewood Cliffs, NJ.
Sammis, C.G., Osborne, R.H., Anderson, J.L., Banerdt, M., White, P., 1986. Self-similar cataclasis in the formation of fault gouge. Pure Appl. Geophys. 124 (1/2), 53–78.
Turcotte, D., 1986. Fractals and fragmentation. J. Geophys. Res. 91 (B2), 1921–1926.
Vesic, A.S., Clough, G.W., 1968. Behaviour of granular materials under high stresses. J. Soil Mech. Found. Div. ASCE 94 (SM 3), 661–688.
Xiao, Y., Liu, H., 2017. Elastoplastic constitutive model for rockfill materials considering particle breakage. Int. J. Geomech. 17 (1), 04016041.
Xiao, Y., Liu, H., Ding, X., Chen, Y., 2016. Influence of particle breakage on critical state line of rockfill material. Int. J. Geomech. 16 (1), 04015031.
Xiao, Y., Long, L., Evans, M., Zhou, M., Liu, H., Stuedlein, A., 2019. Effect of particle shape on stress-dilatancy responses of medium-dense sands. J. Geotech. Geoenviron. Eng. 145 (2), 04018105.
Xiao, Y., Meng, M., Chen, H., He, X., Ran, J., Shi, W., 2018. Nonlinear regression model for peak-failure strength of rockfill materials in general stress space. Geosci. Front. 9 (6), 1699–1709.
Yin, Z.-Y., Hicher, P.-Y., Dano, C., Jin, Y.-F., 2017. Modeling mechanical behavior of very coarse granular materials. J. Eng. Mech. 143 (1). C4016006, 1-11.
Zhang, Y.D., Buscarnera, G., 2017. A rate-dependent breakage model based on the kinetics of crack growth at the grain scale. Géotechnique 67 (11), 953–967.